Electron Transfer of Carotenoids Imbedded in MCM-41 and Ti−MCM-41: EPR, ENDOR, and UV−Vis Studies

Yunlong Gao, Tatyana A. Konovalova, Tao Xu, and Lowell D. Kispert*

Department of Chemistry, Box 870336, University of Alabama, Tuscaloosa, Alabama 35487-0336

Received: April 19, 2002; In Final Form: July 26, 2002

Electron transfer (ET) reactions of carotenoids (Car), β-carotene (**I**), canthaxanthin (**II**), and 7′-apo-7′,7′-dicyano-β-carotene (**III**) imbedded in MCM-41 and Ti−MCM-41 were studied as a function of oxidation potential. The ET efficiency in MCM-41 was highest for the carotenoid with the lowest oxidation potential. The presence of Ti^{4+} in the framework of MCM-41 enhanced the ET efficiency of all carotenoids, but the enhancement did not depend on oxidation potential. The enhancement depends on whether complexes are formed between carotenoids and Ti^{4+}. Complexes were formed with **I** and **III** but not with **II**. The presence of Ti^{4+} results in a large blue shift of the maximum absorption wavelength due to changes in the carotenoid conformation.

Introduction

Photoionization is the first step in many light driven reactions related to the storage of light energy.[1] Electron transfer (ET) reactions within organic assemblies of vesicles and micelles[2−4] and porous inorganic solids such as zeolites[5−9] and silica gels[10−12] have been studied to establish artificial photoredox systems for solar energy conversion and storage.

MCM-41 is a mesoporous silica containing a regular array of uniform linear pores. The pore size ranges from 15 to 100 Å, depending on the chain length of the template used in the synthesis.[13] Previous studies[14−16] have shown that such materials provide an appropriate microenvironment to retard back electron transfer and increase the lifetime of the photoproduced radical ions. The MCM-41 matrix whose framework is modified by incorporating metal ions enhances the electron-accepting ability of the MCM-41 matrix.[14−16] Different metal ions such as Al, Ti, and Ni have been studied and the ET efficiency has been found to depend on both metal ions and dyes. For example,[14,15] the photoyield for photoionization of porphyrins in MCM-41, AlMCM-41, and Ti−MCM-41 increases in the order AlMCM-41 < MCM-41 < Ti−MCM-41; but the photoyield for N-alkylphenothiazines in these materials increases in the order MCM-41 < AlMCM-41 < Ti−MCM-41.

Carotenoids (Car) play important roles in photosynthetic systems as photoprotecting agents and light harvesting antenna pigments.[17,18] The ET reactions of carotenoids in different hosts, such as liposomes,[19] TX100 micelles,[20] and sol gels,[21] have been previously studied by our group. Because Car exists in the polar proteinacous environment in photosystem II, MCM-41 with polar −SiOH groups on the surface is a good artificial host for simulation of proteinacous environments. Recently, the ET reactions of Car in MCM-41, Ni−MCM-41, and AlMCM-41 have been studied.[16] The photoyield for Car imbedded in MCM-41, Ni−MCM-41 and AlMCM-41 increases in the order: MCM-41 < Ni−MCM-41 < AlMCM-41.

In the present study, the ET efficiencies of the carotenoids β-carotene (**I**), canthaxanthin (**II**) and 7′-apo-7′,7′-dicyano-β-carotene (**III**) (see Scheme 1) imbedded in MCM-41 and Ti−MCM-41 were examined. Optical study of the interaction between Car and Ti^{4+} was carried out. It is known that carotenoid radical cation ($Car^{\bullet+}$) and dication (Car^{2+}) can be easily produced in solution by electrolysis[22−26] or by oxidation with $FeCl_3$.[27−29] The ease of oxidation depends on the electron-donating or withdrawing strength of the terminal substituents.[30,31] Because the ease with which dications are produced can be equal to or greater than that of the cation radicals,[32] it is possible that dications along with the cation radicals are also involved in photoprotecting the photosynthetic reaction centers.[33] Whether carotenoid dications can be produced by photoexcitation is unclear. The present study also focuses on this question. The effect of O_2 on ET reactions is discussed in this study.

Experimental Section

Synthesis of MCM-41 and Ti−MCM-41. The procedure used for the preparation of the siliceous material (MCM-41) was similar to that reported by Beck et al.[13] First, tetrabutylammonium silicate (TBAS) was prepared in a 10:1 ratio (w/w) from tetrabutylammonium hydroxide (40 wt %, Aldrich) and fumed silica (Sigma). Then 20.3 g of cetyltrimethylammonium chloride (CTAC, 25 wt %, Aldrich) and 12.21 g of TBAS were mixed with 5.94 g of H_2O. Finally, 5.91 g of fumed silica was dissolved in the mixture. The resulting gel was placed in a Teflon bottle and heated for 6 d at 95 °C, cooled to room temperature, washed with deionized water, and finally dried in air. The template CTAC was removed by calcination in air at 530 °C for 18 h. The resulting white powder is called MCM-41.

Ti−MCM-41 was synthesized according to the method of Maschmeyer et al.[34] A 50 mL aliquot of titanocene dichloride (95 wt %, TCI) in chloroform (10 mM) was added to 0.5 g MCM-41. The titanocene dichloride was allowed to diffuse into MCM-41 for 30 min until the MCM-41 became red. Then a drop of triethylamine was added to the mixture to activate the surface silanols of the MCM-41. The color of the MCM-41 changed from red to orange to yellow over a period of 2 h, signifying that the well-established substitution of chloride by alkoxide/siloxide ligands had occurred. The resulting product

* To whom correspondence should be addressed. E-mail: likspert@bama.ua.edu. Fax: (205) 348-9104.

10.1021/jp025978s CCC: $22.00
Published on Web 09/28/2002

SCHEME 1: Structures of Carotenoids of I, II, and III

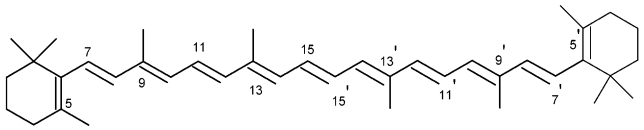

All-trans β-carotene (**I**)

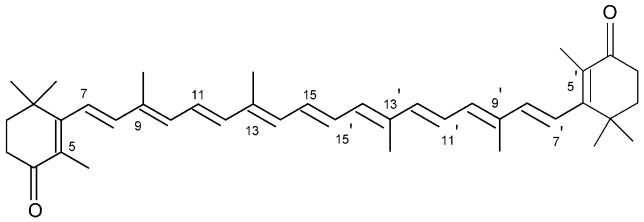

All-trans Canthaxanthin (**II**)

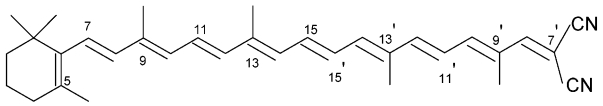

7'-Apo-7', 7'-dicyano-β-carotene (**III**)

was recovered by filtration, washed several times with chloroform, and then the sample was calcinated in a flow of air at 530 °C for 24 h. The resulting white powder is designated Ti−MCM-41. The concentration of Ti^{4+} is about 0.001 mM/mg. According to SEM measurements, the concentration of Si was 0.03 mM/mg and O was 0.06 mM/mg.

Chemicals. All-*trans*-*β*-carotene (**I**) and all-*trans*-canthaxanthin (**II**) were purchased from Fluka. 7′-Apo-7′,7′-dicyano-*β*-carotene (**III**) was synthesized as previously described.[35] Anhydrous dichloromethane was from Aldrich.

EPR Sample Preparation. MCM-41 or Ti−MCM-41 (100 mg) was activated at 200 °C for 6 h, then at once transferred to a N_2 drybox and allowed to cool to room temperature. A 4-mL portion of a 5 mM carotenoid CH_2Cl_2 solution was prepared and added to the above; the carotenoid was allowed to diffuse into the MCM-41 or Ti−MCM-41 matrix for 10 min; the mixture was stirred to evaporate the solvent, and the residue was transferred to an EPR tube, which was then stoppered. The EPR tube was taken out of the drybox, and the residual solvent was removed under vacuum (0.01 Torr). The concentration of Car in the host is about 0.0002 mM/mg or approximately an order of magnitude smaller than the Ti^{4+} concentration and is the limiting reagent. All of the samples were prepared using the same EPR tube, and the same liquid N_2 dewar was used during photoirradiation and the sample was exposed to the same amount of light over a fixed time. Thus, variations in lamp intensity and scattered light have been minimized and below the error in photoyield measurements. The errors are largely due to variation in EPR measurements.

Instrumentation. X-ray powder diffraction (XRD) data were obtained from thin layers of samples, and measurements were carried out with a Philips 1840 diffractometer using Cu Kα radiation ($\lambda = 1.541$ Å) within the scattering angle 2θ range of 1.5−10°.

A S-2500 HITACHI Scanning Electron Microscope (SEM) with TRACOR NOTHERN Energy Dispersive X-ray Analysis Unit was used to measure the concentration of Ti^{4+} in Ti−MCM-41. The X-ray energy used in the measurements was 15 KV.

EPR measurements were carried out with an X-band (9.5 GHz) Varian (Palo Alto, CA) E−12 EPR spectrometer, equipped with a rectangular cavity. The magnetic field was measured with a Bruker (Billerica, MA) EPR 035M gaussmeter, and the microwave frequency was measured with a model HP 5245L frequency counter.

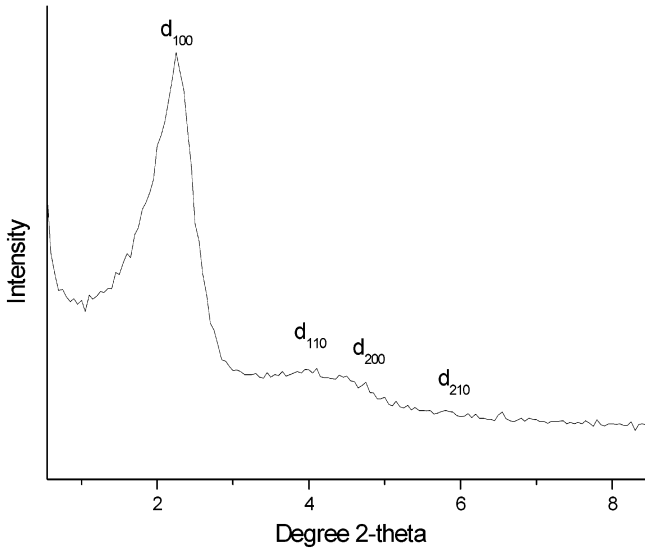

Figure 1. Powder X-ray diffraction pattern of calcined MCM-41.

A 250 W Xenon lamp (ILC Technology) at a distance of 20 cm was used to irradiate the samples. An optical filter was used to cut off most of the UV light below 350 nm. The light intensity was controlled by adjusting the electric current, 10 amperes (A) were used in the irradiation.

A Vydac 201 TP54 polymeric C_{18} column (250 × 4.6 mm i.d.) packed with 5 μm particles (Hesperia, CA) and a Shimadzu LC-600 pump with a SPD-M10AVP PDA detector were used for the HPLC separation and detection.

Optical spectra were recorded with a double beam Shimadzu UV−vis 1601 spectrophotometer (190−1100 nm). MCM-41 and Ti−MCM-41 samples were made into thin films by pressing the samples between two quartz plates so that light can penetrate the samples; then the plates were sealed with tape. For low temperature (77 K) experiments, the samples were sealed with a low temperature-resisting tape and placed in a glass dewar filled with liquid N_2. Ar gas was used to purge the sample chamber of the instrument so that water did not condense on the wall of the dewar.

ENDOR spectra were recorded on a Bruker ESP 300−10/7 EPR spectrometer with an ENDOR accessory.

ZINDO/1[36] and ZINDO/S[37] calculations were performed using Hyperchem 6.03 software on a Dell computer (Pentium 111).

EPR simulation was performed using WINEPR SimFonia version 1.25.

Results and Discussion

MCM-41 and Ti−MCM-41. The XRD pattern of siliceous MCM-41 molecular sieves after calcinations is shown in Figure 1. The XRD pattern of MCM-41 samples is that of a hexagonal lattice as published in the literatures;[38] the intense peak at $2\theta = 2.2°$. According to Bragg's equation,[39] ($2d\sin\theta = \lambda$, $\lambda = 1.5417$ Å for the Cu Kα line), the spacing is about $d_{100} = 40$ Å. Recent accurate measurements by combined XRD/adsorption analysis showed that the pore size of calcined MCM-41 by a template of micellar surfactant with C_{16} chain length is about 38 Å.[40] Thus, there is no problem for carotenoid molecules (chain length, ∼25 Å) to diffuse into such large pores.

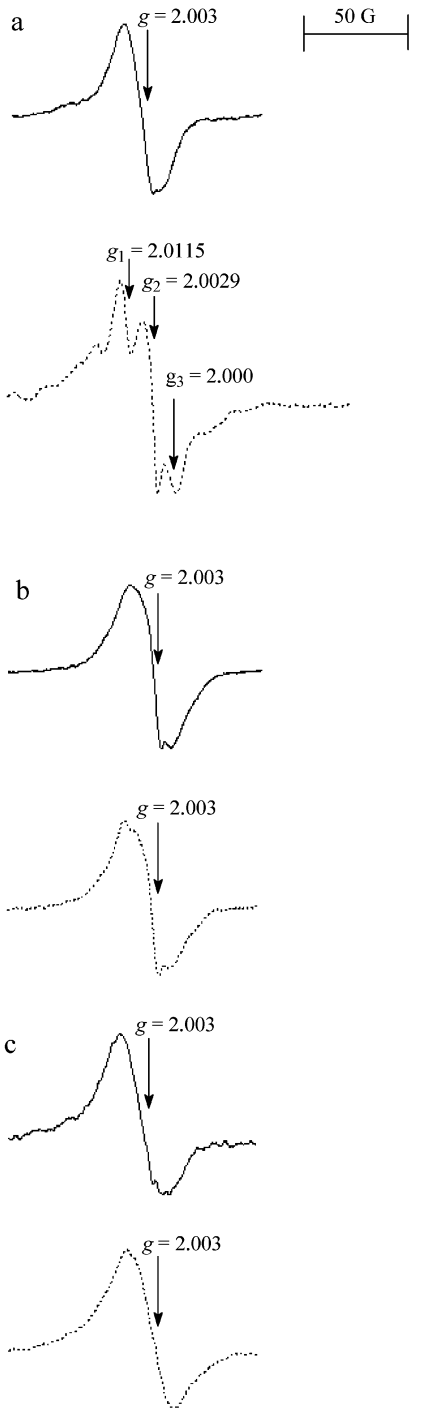

Figure 2. 77 K EPR spectra of sample with **I** (a), **II**, (b) and **III** (c) imbedded in MCM-41. Solid line: after 5 min photoirradiation. Dashed line: after another 5 min irradiation.

Ti−MCM-41 showed the same XRD pattern, indicating that the substitution of Ti^{4+} into the framework of MCM-41 does not alter the structure of MCM-41. The Ti/Si atomic ratio of the Ti−MCM-41 sample was measured by a scanning electron microscope with an energy-dispersive X-ray analysis unit. The ratio is about 0.04.

Electron Transfer in MCM-41. No EPR signal was detected after **I**, **II**, or **III** were imbedded in MCM-41, indicating that no detectable dark reaction occurs. The 77 K EPR spectrum of the sample with **I** imbedded in MCM-41 after 5 min photoirradiation at 77 K is shown in Figure 2a; a broad signal with peak to peak line width (ΔH_{pp}) of 21 G and a g value of 2.003. Because the g value of $Car^{\bullet+}$**(I)** is 2.0028[41,42] and the ΔH_{pp} of $Car^{\bullet+}$**(I)** on solid support is 14.6 G,[43] the broad asymmetric peak is due to overlap of the $Car^{\bullet+}$ signal and other EPR signals. It is known[16,44] that photoirradiation of MCM-41 produces an $O_2^{\bullet-}$ signal so we assume that the peak is due to the overlap of $Car^{\bullet+}$ and $O_2^{\bullet-}$ signals. This assumption becomes more certain after another 5 min photoirradiation of the sample at 77 K. The EPR spectrum is shown as the dashed line. The signal with $g_1 = 2.0115$, $g_2 = 2.0029$ and $g_3 = 2.000$ is characteristic of the $O_2^{\bullet-}$ species generated in MCM-41 ($g_1 = 2.012$, $g_2 = 2.003$ and $g_3 = 2.00$).[16,44] The absence of the $Car^{\bullet+}$ signal is attributed to formation of the dication produced by ET from $Car^{\bullet+}$ to the MCM-41 matrix according to eq 1

$$Car^{\bullet+}\textbf{(I)} - e^- \rightarrow Car^{2+}\textbf{(I)} \quad (1)$$

This assignment is supported by optical detection of the dication formation described later. Because no EPR signal was detected at half field, the species formed is a singlet consistent with the formation of a dication as determined before.[23] All signals disappeared after the sample was warmed to room temperature and measured again at 77 K. Recombination reactions such as (2) and (3) could occur at higher temperature

$$Car^{2+} + O_2^{\bullet-} \rightarrow Car^{\bullet+} + O_2 \quad (2)$$

$$Car^{\bullet+} + O_2^{\bullet-} \rightarrow Car + O_2 \quad (3)$$

There is a possibility that the absence of the $Car^{\bullet+}$ signal after photoirradiation may be due to complete decay of $Car^{\bullet+}$ to other small molecules. To rule out this possibility, the sample, after warming to room temperature, was photoirradiated again at 77 K for 5 min. The EPR spectrum is the same as the solid line in Figure 2a both in shape and intensity. The photoyield of $Car^{\bullet+}$-**(I)** imbedded in MCM-41 after 5 min photoirradiation was measured to be about 30%. It was found that the yield decreases with the decrease in the concentration of Car when the concentration of Car in MCM-41 is less than 0.0002 mM/mg. If the $Car^{\bullet+}$**(I)** completely decays after photoirradiation, then the intensity of $Car^{\bullet+}$ EPR signal after re-photoirradiation should be lower than that of the previous one. This was not observed, and so, the possibility of the complete decay of $Car^{\bullet+}$ under irradiation of the sample is excluded. HPLC was also used to analyze the solution extracted from the EPR sample after 10 min of photoirradiation (CH_2Cl_2 was used as the solvent). No decay products were found.

The 77 K EPR spectrum of the sample with **II** imbedded in MCM-41 after 5 min photoirradiation at 77 K is shown in Figure 2b. A broad signal with ΔH_{pp} of about 22 G and a g value of about 2.003 was detected. Because the g value of $Car^{\bullet+}$**(II)** is 2.0027[41,42] and ΔH_{pp} of $Car^{\bullet+}$**(II)** produced on solid support is 15.4 G,[43] the peak is attributed to overlap of the spectrum of $Car^{\bullet+}$ and that of another species, presumably $O_2^{\bullet-}$. After another 5 min of photoirradiation at 77 K, the EPR spectrum changes slightly. This can be attributed to the change of the intensity ratio of the overlapping species although the EPR signal of $Car^{\bullet+}$ did not disappear completely.

Figure 2c shows the 77 K EPR spectrum of the sample with **III** imbedded in MCM-41 after 5 min photoirradiation at 77 K and that after another 5 min of photoirradiation. The difference between the two spectra is that the intensity of the initial EPR signal is lower than that of the signal after 10 min irradiation.

The simulations of the EPR spectra with different intensity ratios of $O_2^{\bullet-}$ to $Car^{\bullet+}$**(I)** is shown in Figure 3. The simulations agree with the experiment results, i.e., the overlap of $O_2^{\bullet-}$ and

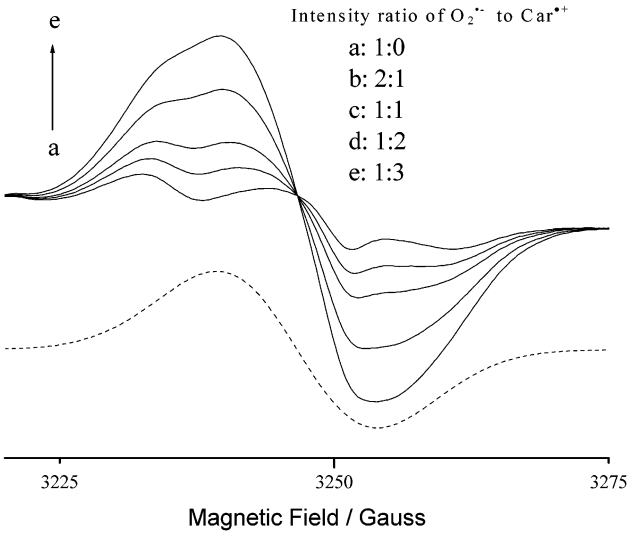

Figure 3. Simulations of the EPR spectra with different intensity ratios of $O_2^{\bullet-}$ to $Car^{\bullet+}$**(I)**. The dashed line is the EPR signal of $Car^{\bullet+}$**(I)** obtained by simulation.

$Car^{\bullet+}$ is broader than that of $Car^{\bullet+}$ and the concentration ratio of $Car^{\bullet+}$ to $O_2^{\bullet-}$ increases from 3a to 3e.

To compare the ET efficiency for the three compounds imbedded in MCM-41, the integrated values of the EPR signals (solid lines) in Figures 2a,b,c were compared. The ET efficiency of **I** is much higher than those of **II** and **III**, and that of **II** is comparable to that of **III**. The much higher ET efficiency of **I** may be attributed to the fact that **I** has the lowest oxidation potential due to the electron donating substituents (0.6 vs 0.8 V) and **I** has an inversion of oxidation potentials,[32] so dications are formed at a lower potential than that for radical cations. The first oxidation potentials (vs SCE) for **I**, **II**, and **III** in CH_2Cl_2 are 0.63,[32] 0.77,[32] and 0.79 V,[45] respectively; the second oxidation potentials (vs SCE) for **I**, **II**, and **III** are 0.60,[32] 0.97,[32] and 0.97 V,[45] respectively. The inversion of oxidation potentials in the oxidation of **I** is due to the weakening of the Coulombic repulsion which occurs when the two charges of the dication are localized at the end of **I**, at a large distance from one another.[32] This localization is favored by the ease of oxidation of the terminal groups of **I**. Localization of the charges in the dication of **I** contributes to its stabilization due to the effect of solvation, whereas the delocalization of the charge over the whole molecular framework in the cation radical decreases its stabilization due to solvation.[32] This explains why the formation of Car^{2+}**(I)** by photoirradiation is much easier than the dication of **II** or **III**.

Electron Transfer in Ti−MCM-41. No EPR signal was detected after **I**, **II**, or **III** were imbedded in Ti−MCM-41, indicating that no detectable dark reaction occurs. Figure 4a shows the 77 K EPR spectrum of the sample with **I** imbedded in Ti−MCM-41 after 5 min photoirradiation at 77 K. A broad peak with ΔH_{pp} about 22 G and g value about 2.003 was detected. After another 5 min of photoirradiating the sample at 77 K, the EPR signal formed is shown as a dashed line with $g_1 = 2.021$, $g_2 = 2.008$ and $g_3 = 2.001$ characteristic of a $Ti^{4+}(O_2^{\bullet-})$ species.[46,47] Another signal at high field is also observed with $g_\perp = 1.959$ and $g_\parallel = 1.903$ similar in g values ($g_\perp = 1.958$ and $g_\parallel = 1.902$) to that of Ti^{3+} produced in Ti−MCM-41 by hydrogen reduction.[47] As in Figure 2b, the initial broad peak formed after 5 min of irradiation is due to the overlap signals of $Car^{\bullet+}$ and $Ti^{4+}(O_2^{\bullet-})$. It was reported that $Ti^{4+}(O_2^{\bullet-})$ in Ti−MCM-41 is produced by γ-irradiation[46] or reduction with hydrogen.[47] The reaction mechanism[47] is cleavage of one Ti−O bond during the reduction process forming a Ti^{3+} species. The latter on reoxidation with O_2 forms $Ti^{4+}(O_2^{\bullet-})$. The O_2 effect on the ET reaction was examined by preparing the EPR sample under low vacuum (1 Torr) (instead of 0.01 Torr) and repeating the experiment. Only the strong $Ti^{4+}(O_2^{\bullet-})$ signal is detected and the Ti^{3+} signal was not detected, indicating that Ti^{3+} reacts with O_2 to form $Ti^{4+}(O_2^{\bullet-})$. The Ti^{3+} signal was not detected after the first 5 min photoirradiation because Ti^{3+} reacts with O_2 to form $Ti^{4+}(O_2^{\bullet-})$. Ti^{3+} is detected only after O_2 is consumed. Complete remove of O_2 from the sample is difficult. A previous study[47] has shown that even the EPR sample prepared under 0.001 Torr, a significant amount of O_2 still exists in the sample.

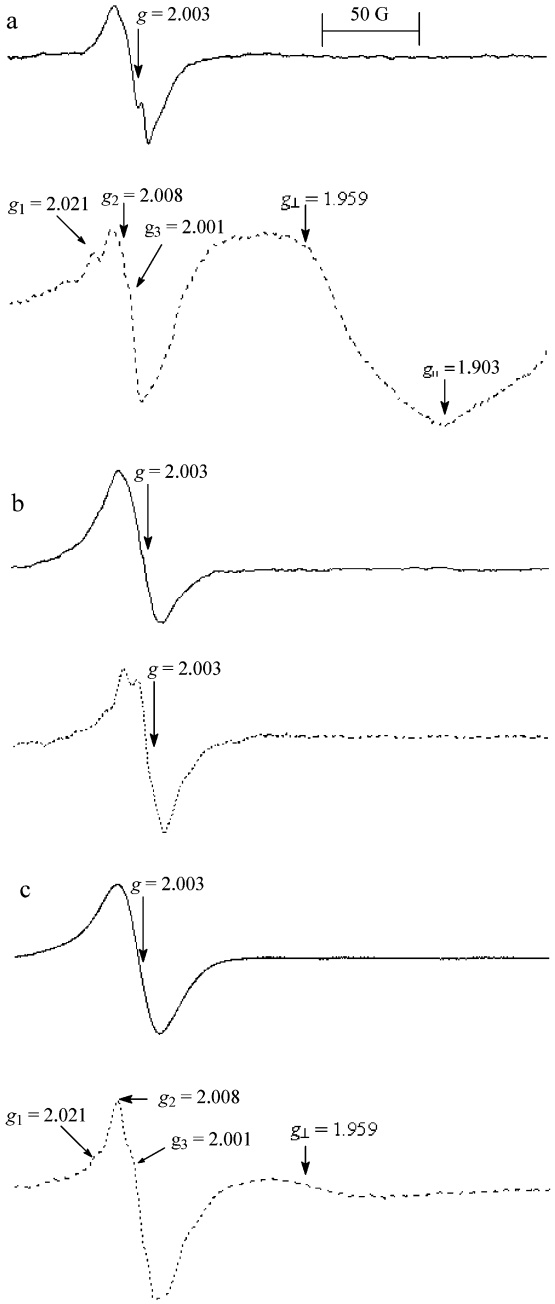

Figure 4. 77 K EPR spectra of sample with **I** (a), **II**, (b) and **III** (c) imbedded in Ti−MCM-41. Solid line: after 5 min photoirradiation. Dashed Line: after another 5 min irradiation.

The 77 K EPR spectrum of the sample with **II** imbedded in Ti−MCM-41 after 5 min of photoirradiation at 77 K is shown in Figure 4b. A broad peak due to overlap of $Car^{\bullet+}$**(II)** and

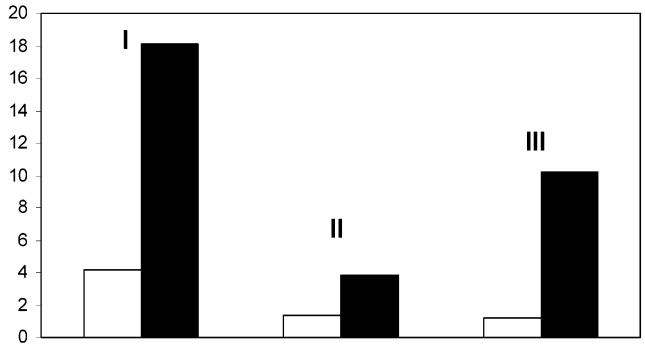

Figure 5. Photoyield comparison of **I**, **II**, and **III** inbedded in MCM-41 and Ti−MCM-41. Blank columns represent photoyield in MCM-41; Black columns represent that in Ti−MCM-41. Error in photoyield measurements is estimated to be ±10%.

$Ti^{4+}(O_2^{\bullet-})$ signals was detected. After another 5 min of photo irradiation at 77 K, the spectrum shown as a dashed line changes significantly due to an increase of the $Ti^{4+}(O_2^{\bullet-})$ signal and a decrease of the $Car^{\bullet+}$ signal. The $Car^{\bullet+}$ signal does not completely disappear, consistent with the relative difficulty of forming the dication of **II** relative to **I**.

The 77 K EPR signal of the sample with **III** imbedded in Ti−MCM-41 after 5 min photoirradiation at 77 K is shown in Figure 4c. After another 5 min photoirradiation, the $Ti^{4+}(O_2^{\bullet-})$ signal with $g_1 = 2.021$, $g_2 = 2.008$, and $g_3 = 2.001$ shown as a dashed line was detected. The $Car^{\bullet+}$ signal is no longer detectable. The Ti^{3+} signal $g_\perp = 1.959$ was also detected ($g_{||}$ signal was too weak to be observed).

Figure 5 shows the comparison of the photoyields of **I**, **II**, and **III** imbedded in Ti−MCM-41 with MCM-41. The comparison shows that introduction of Ti^{4+} into the MCM-41 framework enhances the ET effiency significantly for all carotenoids studied here, but the enhancements are different for different carotenoids. A greater enhancement occurs for **I** and **III** compared with that for **II**.

Optical Study. UV−vis transmission spectra for **I**, **II**, and **III** imbedded in MCM-41 and Ti−MCM-41 are shown in Figure 6. Because the samples were thin films, the spectral lines are irregular due to light diffraction. The three vibronic bands characteristic of long chain polyenes are not resolved due to broadening of these bands in a polar environment.[48] The maximum absorption wavelengths (λ_{max}) of **I**, **II**, and **III** in MCM-41 are 490, 530, and 570 nm, respectively, and show a large red shift compared with that in solvents such as CH_2Cl_2 (λ_{max} of **I**, **II**, and **III** in CH_2Cl_2 are 460, 481, and 555 nm, respectively). This phenomenon agrees with Andersson et al.'s study[49] that the large red-shifted absorbance of Car in the polar proteinous environment is due to mutual polarizability interactions between the Car and the surrounding medium. For **I** and **III** imbedded in Ti−MCM-41, λ_{max} shows a significant blue shift compared with that in MCM-41(60 nm for **I**; 20 nm for **III**), indicating that **I** and **III** interact with Ti^{4+}. There are two types of interactions[50] between unsaturated compounds and transition metal ions: coordination (overlap of the delocalized π-electron density of the unsaturated compound and the d orbital of the transition metal ion) and electrostatic interaction. For the Ti ion, coordination is the main interaction.[50] No significant change was found for **II** (the difference in λ_{max} is in the measurement error range), indicating that **II** does not interact with Ti^{4+}.

The blue shift of λ_{max} of Car can be explained by a change in the π-conjugation along the Car conjugated chain due to the conformation change when Car interacts with Ti^{4+}. For example,[51] an optical study of the absorption spectra of a C_{30} spheroidene and β-apo-12′-carotene in a mixture of solvents (ether/isopentane/ethanol, 5/5/2, v/v/v) shows that the spectrum of β-apo-12′-carotene is significantly blue shifted compared to that of spheroidene although they both contain seven conjugated double bonds. The explanation[51] for this phenomenon is that the spheroidene enjoys the full effect of seven conjugated double bonds, whereas the effective conjugation length of β-apo-12′-carotene is less than seven conjugated double bonds because the double bond in the ring (C5−C6) is out of the plane formed by other carbon−carbon double bonds due to the repulsions between methyl groups on the ring and the hydrogen atom at the end of the C7−C8 double bond. We performed ZINDO/S calculations[37] to examine the UV−vis spectra of the Car and its complex with Ti^{4+}. The singly excitation configuration interaction involving about 100 configurations was used to calculate the optical absorption spectrum. ZINDO/1[36] was used to optimize the geometries and restricted Hartree−Fock (RHF) formalism was used in the optimization processes. A series of complex conformations was obtained depending on the initial position of Ti^{4+} around the conjugated chain of Car during the geometry optimization. Figure 7 shows the geometries of **I** and

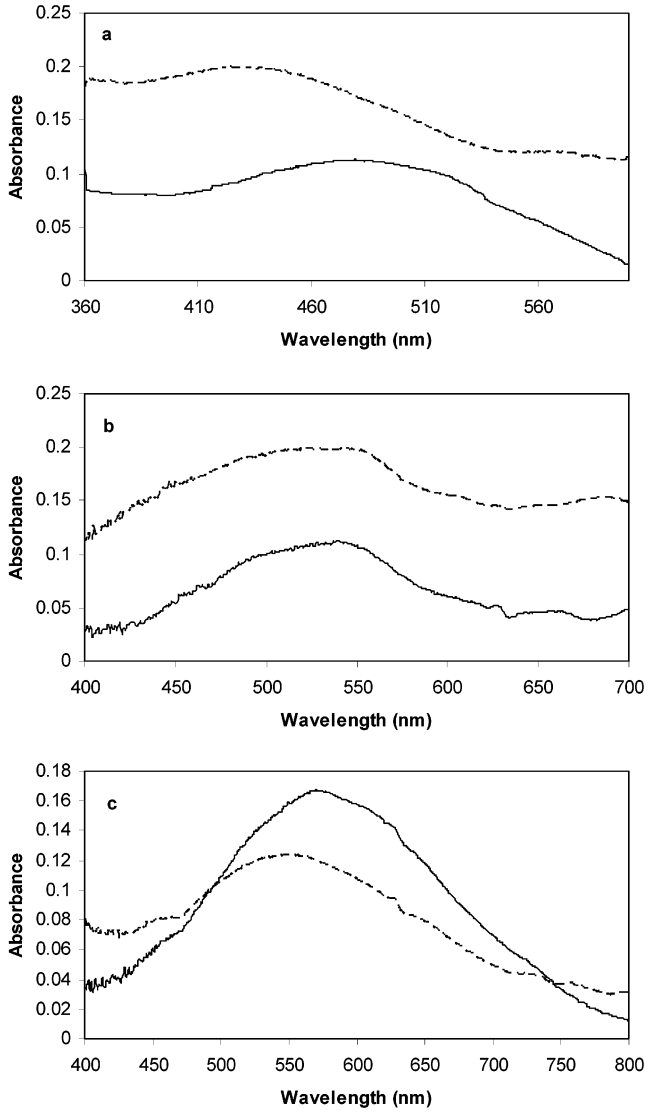

Figure 6. UV−vis spectra of **I**, **II**, and **III** imbedded in MCM-41 and Ti−MCM-41. (a) **I**, (b) **II**, and (c) **III**. Solid line is that for Car imbedded in MCM-41 and dashed line is that for Car imbedded in Ti−MCM-41.

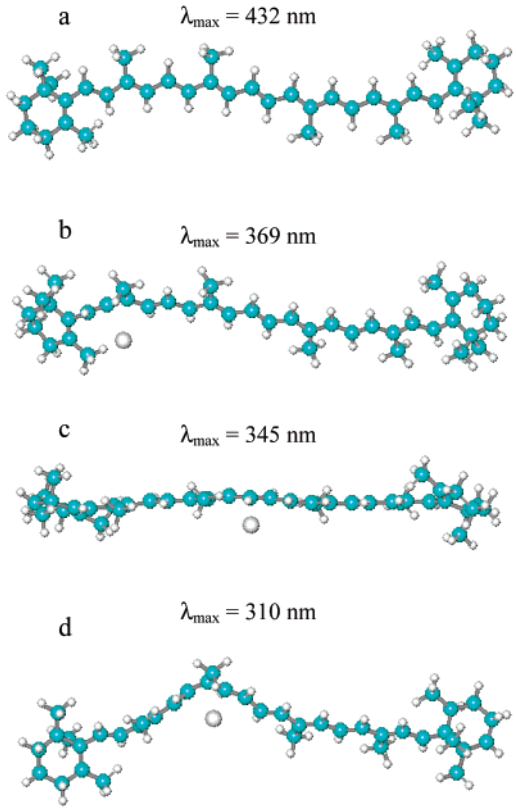

Figure 7. Geometries of **I** and complexes of **I** and Ti^{4+} by ZINDO/1 geometry optimizations. (a) **I**, (b)−(d): complexes obtained with the initial position of Ti^{4+} located near C7−C8, C15−C15′, and C13−C14 double bonds, respectively. The λ_{max} of the strongest peak is calculated by ZINDO/S.

three complexes of **I** and Ti^{4+}. The λ_{max} of the strongest peak calculated by ZINDO/S was also shown in Figure 7. For complexes, the carotenoid chain distorts to various degrees depending on the location of Ti^{4+}. The distortion is represented by a change in torsion angles. These changes are more significant near Ti^{4+}. For example, the torsion angle of C7−C8−C9−C10 for the geometry in Figure 7b. changes from 178.5° to 133.9°, the torsion angle of C13−C14−C15−C15′ for the geometry in Figure 7c changes from 178.9° to 171.8° and the torsion angle of C11−C12−C13−C14 for the geometry in Figure 7d changes from 175.9° to 126.4°. The bond length also changes. It was reported[52] that the distortion of π conjugated system causes the rehybridization of carbon and thus causes the bond length change. For example, the C7−C8 double bond and C8−C9 single bond in Figure 7a changes from 1.353 to 1.462 Å and from 1.453 to 1.355 Å, respectively; the C15−C15′ double bond and C14−C15 single bond in Figure 7b changes from 1.358 to 1.420 Å and from 1.437 to 1.382 Å, respectively; the C13−C14 double bond and C12−C13 single bond changes from 1.366 to 1.423 Å and from 1.448 to 1.401 Å, respectively. UV−vis spectra of Car and the complexes obtained by ZINDO/S calculation show that λ_{max} of the strongest peak of the complexes is blue shifted compared to that of Car. The magnitude of the shift depends on the location of Ti^{4+}. For **I**, the blue shift can be more than 100 nm. This result agrees with the calculations of Chen et al.[53] that for a π-conjugated polymer, the transition energy increases with a decrease of π-conjugation (from planar conformation to nonplanar conformation).

The higher ET efficiencies for **I** and **III** imbedded in Ti−MCM-41 can be attributed to the formation of a complex. The

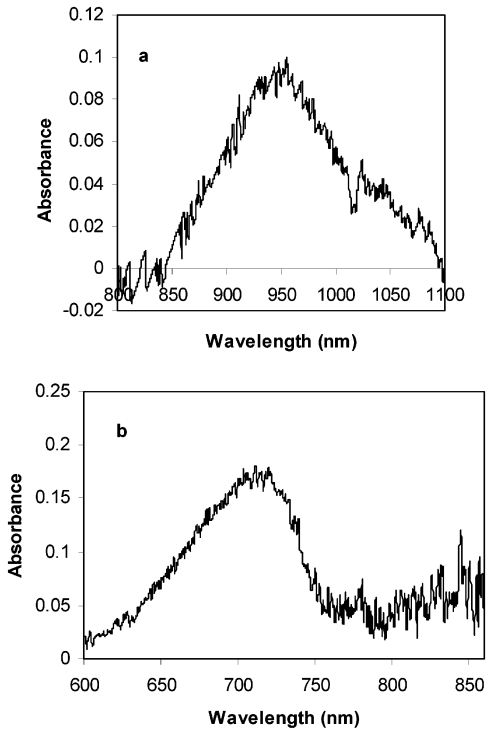

Figure 8. UV−vis spectra of $Car^{\bullet+}$ and Car^{2+} of **I** produced by photoirradiation at 77 K and recorded at 77 K. (a) UV−vis spectrum of $Car^{\bullet+}$, baseline corrected. (b) UV−vis spectrum of Car^{2+}, baseline corrected.

decrease in the distance between the Car chain and Ti^{4+} favors the electron transfer. Recently, it was proposed that the photon-induced ET efficiency from a dye to a electrode increases significantly with a decrease in distance between the mainframe of the dye molecule and the electrode.[54−56] A possible explanation[57] is that if the electron-transfer time is longer than the excited-state lifetime of the dye, the electron transfer is not successful.

Figure 8a shows the UV−vis spectrum from 800 to 1100 nm of $Car^{\bullet+}$(**I**) after 10 s photoirradiation at 77 K. The λ_{max} in Figure 8a is about 950 nm which shows a 50 nm blue shift compared with that of $Car^{\bullet+}$(**I**) generated by electrolysis in CH_2Cl_2.[28] Normally. the UV−vis spectrum of Car shows a broad peak with a maximum at 450 nm and no other peaks. The formation of $Car^{\bullet+}$ and Car^{2+} in CH_2Cl_2 are indicated by peaks appearing around 1000 or 800 nm respectively. According to the previous ZINDO/S calculations and optical studies by our group,[28] the dication peak should appear between those of Car and $Car^{\bullet+}$. Figure 8b shows the UV−vis spectrum of Car^{2+}(**I**) after 10 s of photoirradiation at 77 K. The λ_{max} is about 720 nm which shows a blue shift of about 90 nm compared with that of Car^{2+} generated by oxidation with $FeCl_3$ in CH_2Cl_2.[28] The large blue shifts of λ_{max} of $Car^{\bullet+}$ and Car^{2+} may be attributed to the formation of a contact ion pair (CIP) between these species and $Ti^{4+}(O_2^{\bullet-})$. The ZINDO/S calculation[57] shows that the formation of CIP between $Car^{\bullet+}$ and counteranion can cause a large blue shift in the λ_{max} of $Car^{\bullet+}$. The polar environment of MCM-41 may also cause a large blue shift in the λ_{max} of $Car^{\bullet+}$ and Car^{2+}. For example,[58] the λ_{max} of $Car^{\bullet+}$-(**I**) in aqueous TX-100 micelles is 936 nm.

ENDOR Study

The orientation of $Car^{\bullet+}$ on a solid support can be studied by ENDOR.[16,43] The ENDOR features for methyl group proton

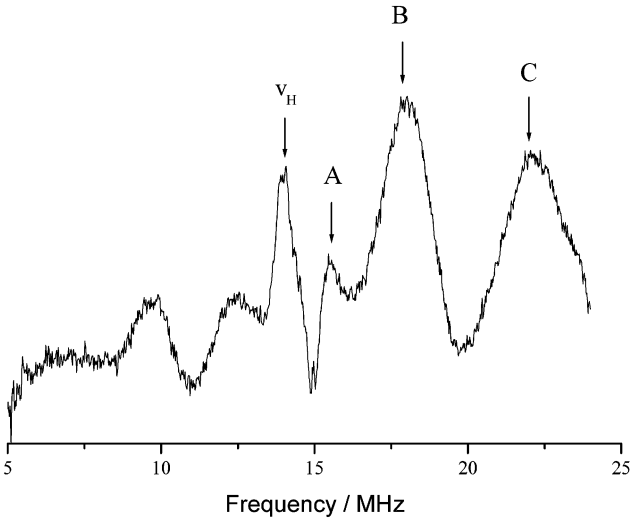

Figure 9. ^{1}H ENDOR spectrum of Car$^{\bullet+}$ of **II** in Ti−MCM-41.

couplings appear as unresolved, very weak and difficult to detect signals in cases where the methyl group is located close to the surface of a matrix. This is due to the large anisotropy of the methyl group protons (line broadening from incomplete averaging of the methyl proton couplings). Figure 9 shows the 120 K ENDOR spectrum of Car$^{\bullet+}$**(II)** in Ti−MCM-41. Peaks A, B, and C are due to the CH_3 proton couplings[16] at C (5 and 5′), C (9 and 9′) and C (13 and 13′) CH_3 protons, respectively. In contrast, an ENDOR spectrum of **I** and **III** in Ti−MCM-41 (not shown) consisted of an unresolved broad line of low intensity. These observations indicate that the conjugated chain of **II** is far away from the surface of the pore, whereas the conjugated chains for **I** and **III** are located near the surface of the pore. This result can explain why **II** does not interact with Ti^{4+}, whereas **I** and **III** do react with Ti^{4+}. The oxygen atom in the cyclohexene ring of **II** may H-bond to the −SiOH group on the surface of the solid hosts with the methyl groups in the ring causing the chain to be located away from the surface of the pore. The CN substituent of **III** may also H-bond to the −SiOH group on the surface but the chain can still interact with the surface.

Conclusions

The photoinduced ET efficiency of carotenoids imbedded in MCM-41 is much higher for Car with no electron-withdrawing group such as for **I** than those with electron-withdrawing groups such as for **II** and **III**. The low oxidation potential for the formation of the carotenoid radical and dication of **I** results in this trend.

The introduction of Ti^{4+} into the MCM-41 framework enhances the photoinduced ET efficiency of Car due to the strong electron-accepting ability of T_i^{4+}, but does not depend significantly on a variation in oxidation potential for different Car. The enhancement is higher for carotenoids which can form complexes with Ti^{4+}. Formation of a complex causes a large blue shift of the λ_{max} of Car due to the conformation change of Car. This is an important result because twisting was found for Car bound to reaction centers.[59] O_2 present in the Ti−MCM-41 also plays an important role in the ET reactions.

The present studies show that the interaction between dye molecule and metal ion must be considered during the study of ET of a dye imbedded in metal ion substituted hosts. The effect of O_2 also cannot be ignored. This study shows some indirect evidences that Car^{2+} can be produced by photoirradiation.

Acknowledgment. Dr. Langqiu Xu (Argonne National Laboratory) and Dr. Larry Kevan (Chemistry Department, U. of Houston) are thanked for supplying suggestions for synthesizing MCM-41 and Ti-MCM-41. Ms. Jolanta Nunley (Biological Sciences Department, U. of Alabama) is thanked for the SEM measurement. Dr. Rainer Schad is thanked for the XRD measurement. Dr. Elli Hand is thanked for helpful discussions. This work was supported by the Chemical Sciences, Geosciences and Biosciences Division, Office of Basic Energy Sciences, Office of Science, U.S. Department of Energy under Grant No. DE-FG02-86ER 13465.

References and Notes

(1) Kevan, L. In *Photoinduced Electron-Transfer Part B*; Fox, M. A., Chanon, M., Eds.; Elsevier: Amsterdam, 1988; p 329.

(2) (a) Fendler, J. H. *Acc. Chem. Res*. **1980**, *13*, 7. (b) Infelta, P. P.; Grätzel , M.; Fendler, J. H. *J. Am. Chem. Soc*. **1980**, *102*, 1479. (c) Dewey, T. G.; Hammes, G. G. *Biophys. J*. **1980**, *32*, 1023. (d) Pileni, M. P. *Chem. Phys. Lett*. **1980**, *71*, 317. (e) Hurst, J. K.; Lee, L. Y. C.; Grätzel, M. *J. Am. Chem. Soc*. **1983**, *105*, 7048.

(3) (a) Kevan, L. In *Photoinduced Electron Transfer, Part B*; Fox, M. A., Chanon, M., Eds.; Elsevier: Amsterdam, 1988; pp 329−384. (b) Kevan, L. *Int. Re*V. *Phys. Chem*. **1990**, *9*, 307. (c) Kevan, L. *Radiat. Phys. Chem*. **1991**, *37*, 629.

(4) (a) McManus, H. J.; Kang, Y. S.; Kevan, L. *J. Phys. Chem*. **1992**, *96*, 5622. (b) Kang, Y. S.; McManus, H. J.; Kevan, L. *J. Phys. Chem*. **1993**, *97*, 2027. (c) Lanot, M. P.; Kevan, L. *J. Phys. Chem*. **1991**, *95*, 10 178. (d) Chastenet de Castaing, E.; Kevan, L. *J. Phys. Chem*. **1991**, *95*, 10 178. (e) Kang, Y. S.; Kevan, L. *J. Phys. Chem*. **1994**, *98*, 4389. (f) Sung-Suh, H. M.; Kevan, L. *J. Phys. Chem. A* **1997**, *101*, 1414. Goncalves, J. A. S.; Gladden, L. F. *J. Phys. Chem*. **1996**, *100*, 390.

(5) Breck, D. W. *Zeolite Molecular Sieves*; Wiley: New York, 1974.

(6) (a) Persaud, L.; Bard, A. J.; Campion, A.; Fox, M. A.; Mallouk, T. E.; Webber, S. E.; White, J. M. *J. Am. Chem. Soc*. **1987**, *109*, 7309. (b) Kim, Y. I.; Mallouk, T. E. *J. Phys. Chem*. **1992**, *96*, 2879. (c) Yoon, K. B. *Chem. Rev*. **1993**, *93*, 321.

(7) (a) Dutta, P. K.; Incavo, J. A. *J. Phys. Chem*. **1987**, *91*, 4443. (b) Incavo, J. A.; Dutta, P. K. *J. Phys. Chem*. **1987**, *91*, 4443. (c) Borja, M.; Dutta, P. K. *Nature* **1993**, *362*, 43. (d) Ledney, M.; Dutta, P. K. *J. Am. Chem. Soc*. **1995**, *117*, 7687.

(8) Faulkner, L. R.; Suib, S. L.; Renschler, C. L.; Green, J. M.; Bross, P. R. In *Chemistry in Energy Production*; Wymer, R. G., Keller, O. L., Eds.; American Chemical Society: Washington, DC, 1982; pp 99−113.

(9) (a) Stamires, D. N.; Turkevich, J. *J. Am. Chem. Soc*. **1964**, *86*, 749. (b) Dollish, F. R.; Hall, W. K. *J. Phys. Chem*. **1967**, *71*, 1005. (c) Kurita, Y.; Sonoda, T.; Sato, M. *J. Catal*. **1970**, *19*, 82. (d) Slinkin, A. A.; Kucherov, A. V.; Kondrat'ev, D. A.; Bondarenko, T. N.; Rubinshtein, A. M.; Minachev, K. M. *J. Mol. Catal*. **1986**, *35*, 97.

(10) (a) Vansant, E. F.; Van Der Voort, P.; Vrancken, K. C. *Characterization and Chemical Modification of the Silica Surface*; Studies in Surface Science and Catalysis, Vol. 93; Elsevier: Amsterdam, 1995. (b) Scott, R. P. W. *Silica Gel and Bonded Phases*; Wiley: Chichester, 1993; Chapters 4 and 6.

(11) (a) Slama-Schwok, A.; Ottolenghi, M.; Avnir, D. *Nature* **1992**, *355*, 240. (b) Slama-Schwok, A.; Avnir, D.; Ottolenghi, M. *J. Am. Chem. Soc.* London, 1973; Vol. 1, Chapter 9. **1991**, *113*, 3984. (c) Marro, M. A. T.; Thomas, J. K. *J. Photochem. Photobiol. A*: *Chem*. **1993**, *72*, 251. (d) Bauer, R. K.; Borenstein, R.; De Mayo, P.; Okada, K.; Rafalska, M.; Ware, W. R.; Wu, K. C. *J. Am. Chem. Soc*. **1982**, *104*, 4635. (e) Wilkinson, F.; Worrall, D. R.; Williams, S. L. *J. Phys. Chem*. **1995**, *99*, 6689.

(12) (a) Xiang, B.; Kevan, L. *Colloid Surf. A* **1993**, *72*, 11. (b) Xiang, B.; Kevan, L. *Langmuir* **1994**, *10*, 2688. (c) Matsuura, K.; Kevan, L. *J. Phys. Chem*. **1996**, *100*, 10 652.

(13) Beck, J. S.; Vartuli, J. C.; Roth, W. J.; Leonowicz, M. E.; Kresge, C. T.; Schmit, K. D.; Chu, T.-W.; Olson, D. H.; Shepperd, E. W.; McCullen, S. B.; Higgins, J. B.; Schlenker, J. L. *J. Am. Chem. Soc*. **1992**, *114*, 10 834.

(14) Krishna, R. M.; Prakash, A. M.; Kevan, L. *J. Phys. Chem. B* **2000**, *104*, 1796.

(15) Sung-Suh, H. M.; Luan, Z.; Kevan, L. *J. Phys. Chem. B* **1997**, *101*, 10 455.

(16) Konovalova, T. K.; Gao, Y.; Schad, R.; Kispert, L. D.; Saylor, C. A.; Brunel, L.-C.*J. Phys. Chem. B* **2001**, *105*, 7459.

(17) Goedheer, J. C. *Annu. Rev. Plant Physiol*. **1972**, *21*, 87.

(18) Koyama, Y. *J. Photochem. Photobiol*. **1991**, *B9*, 265.

(19) He, Z.; Kispert, L. D.; Metzger, R. M.; Gosztola, D.; Wasielewski, M. R. *J. Phys. Chem. B*, **2000**,*104*, 6302.

(20) He, Z.; Kispert, L. D. *J. Phys. Chem*. **1999**, *103*, 9038.

(21) He, Z.; Dissertation of The University of Alabama.

(22) Mairanovsky, V. G.; Engovatov, A. A.; Ioffe, N. T.; Samokhvalov, G. I. *J. Electroanal. Chem.* **1975**, *66*, 123.
(23) Grant, J. L.; Krammer, V. J.; Ding, R.; Kispert, L. D. *J. Am. Chem. Soc.* **1988**, *110*, 2151.
(24) Khaled, M.; Hadjipetrou, A.; Kispert, L. D.; Allendoerfer, R. D. *J. Phys. Chem.* **1991**, *95*, 2438.
(25) Jeevarajan, A. S.; Khaled, M.; Kispert, L. D. *J. Phys. Chem*. **1994**, *98*, 7777.
(26) Jeevarajan, A. S.; Khaled, M.; Kispert, L. D. *Chem. Phys. Lett.* **1994**, *225*, 340.
(27) Wei, C. C.; Gao, G.; Kispert, L. D.; *J. Chem. Soc., Perkin Trans.* **1997**, *2*, 783.
(28) Jeevarajan, J. A.; Wei, C. C.; Jeevarajan, A. S.; Kispert, L. D. *J. Phys. Chem.* **1996**, *100*, 5637.
(29) Krawczyk, S. *Chem. Phys*. **1998**, *230*, 297.
(30) Jeevarajan, A. S.; Khaled, M.; Kispert, L. D. *J. Phys. Chem*. **1994**, *98*, 7777.
(31) Jeevarajan, A. S.; Khaled, M.; Kispert, L. D. *Chem. Phys. Lett.* **1994**, *225*, 340.
(32) Hapiot, P.; Kispert, L. D.; Konovalov, V. V.; Savéant, J.-M. *J. Am. Chem. Soc*. **2001**, *123*, 6669.
(33) Jeevarajan, J. A.; Wei, C. C.; Jeevaranjan, A. S.; Kispert, L. D. *J. Phys. Chem.* **1996**, *100*, 5637.
(34) Maschmeyer, T.; Rey, F.; Sankar, G.; Thomas, J. M. *Nature* **1995**, *378*, 159.
(35) Hand, E. S.; Belmore, K. A.; Kispert, L. D. *J. Chem. Soc., Perkin Trans.* **1993**, *2*, 659.
(36) (a) Bacon, A. D.; Zerner, M. C. *Theor Chim Acta* **1979**, *53*, 21. (b) Zerner, M. C.; Loew, G. H.; Kirchner, R. F.; Mueller-Westerhoff, U. T. *J. Am. Chem. Soc.* **1980**, *102*, 589. (c) Anderson, W. P.; Edwards, W. D.; Zerner, M. C. *Inorg. Chem.* **1986**, *25*, 2728. (d) Culberson, J. C.; Knappe, P.; Rosch, N.; Zerner, M. C. *Theor Chim Acta* **1987**, *71*, 21. (e) Baker, J. D.; Zerner, M. C. *J. Phys. Chem.* **1990**, *94*, 2866. (f) Anderson, W.; Cundari, T.; Zerner, M. C. *Int. J. Quantum Chem*. **1990**, *39*, 31. (g) Anderson, W.; Cundari, T.; Drago, R.; Zerner, M. C. *Inorg. Chem.* **1991**, *29*, 1.
(37) (a) Ridley, J.; Zerner, M. C. *Theor. Chim. Acta* **1973**, *32*, 111. (b) Ridley, J.; Zerner, M. C. *Theor. Chim. Acta* **1976**, *42*, 223.
(38) (a) Kresge, C. T.; Leonowicz, M. E.; Roth, W. J.; Vartuli, J. C.; Beck, J. S. *Nature* **1992**, *359*, 710. (b) Beck, J. S.; Vartuli, J. C.; Roth, W. J.; Leonowicz, M. E.; Kresge, C. T.; Schmitt, K. D.; Chu, C. T.-W.; Olson, D. H.; Sheppard, E. W.; McCullen, B.; Higgins, J. B.; Schlenker, J. L. *J. Am. Chem. Soc*. **1992**, *114*, 10 834. (c) Beck, J. S.; Vartuli, J. C.; Kennedy, G. J.; Kresge, C. T.; Roth, W. J.; Schramm, S. E. *Chem. Mater*. **1994**, *6*, 1816. (d) Vartuli, J. C.; Schmitt, K.; Kresge, C. T.; Roth, W. J.; Leonowicz, M. E.; McCullen, B.; Hellring, S. D.; Beck, J. S.; Schlenker, J. L.; Olson, D. H.; Sheppard, E. W. In *Zeolites and Related Microporous Materials*: *State of the Art 1994*; Weitkamp, J., Karge, H. G., Pfeifer, H., Holderich, W., Eds.; Studies in Surface Science and Catalysis, Vol. 84; Elsevier: Amsterdam, 1994; pp 53−60.
(39) Cullity, B. D. *Elements of X-ray Diffraction* Addison-Wesley: Reading, MA, 1987, P87.
(40) Kruk, M.; Jaroniec, M.; Sakamoto, Y.; Terasaki, O.; Ryoo, R.; Ko, C. H. *J. Phys. Chem. B* **2000**, *104*, 292.
(41) Jeevarajan, A. S.; Khaled, M.; Kispert, L. D. *J. Phys. Chem.* **1994**, *98*, 7777.
(42) Jeevarajan, A. S.; Khaled, M.; Kispert, L. D. *Chem. Phys. Lett.* **1994**, *225*, 340.
(43) Jeevaranjan, A. S.; Kispert, L. D.; Piekara-Sady, L. *Chem. Phys. Lett.* **1993**, *209*. 269.
(44) Chang, Z.; Zhu, Z.; Kevan, L. *J. Phys. Chem. B* **1999**, *103*, 9442.
(45) Jeevarajan, J. A.; Kispert, L. D. *J. Electroanal. Chem*. **1996**, *411*, 57.
(46) Prakash, A. M.; Sung-Suh, H. M.; Kevan, L. *J. Phys. Chem. B* **1998**, *102*, 857.
(47) Bal, R.; Chaudhari, K.; Srinivas, D.; Sivasanker, S.; Ratnasamy, P. *J. Mol. Cata. A* **2000**, *162*, 199.
(48) O'Neil, M. P.; Wasielewski, M. R.; Khaled, M. M.; Kispert, L. D. *J. Chem. Phys.* **1991**, *95*, 7212.
(49) Andersson, P. O.; Gillbro, T.; Ferguson, L.; Cogdell, R. *J. Photochem. Photobio.* **1991**, *54*, 353.
(50) Sodupe, M.; Bauschlicher, C. W. J.; Langhoff, S. R.; Partridge, H. *J. Phys. Chem.* **1992**, *96*, 2118.
(51) Frank, H. A.; Young, A. J.; Britton, G.; Cogdell, R. J. *The Photochemistry of Carotenoids*; Kluwer Academic Publishers: The Netherlands, 1999; pp 223−234.
(52) (a) Yang, X.; Wang, G.; Yang, Z.; Shang, Z.; Cai, Z.; Pan, Y.; Wu, B.; Zhao, X. *J. Mol. Struct.* (*THEOCHEM*) **2002**, *579*, 91. (b) Kovacek, D.; Margetic, D.; Maksic, Z. B. *J. Mol. Struct.* (*THEOCHEM*) **1993**, *285*, 195. (c) Jursic, B. S. *J. Mol. Struct.* (*THEOCHEM*) **1999**, *492*, 85. (d) Mittendorfer, F.; Hafner, J. *Surf. Sci.* **2001**, *472*, 133. (e) Eckert-Maksić, M.; Hodošček, M. Kovaček, D. Maksić, Z. B. Poljanec, K. *Chem. Phys. Lett.* **1990**, *171*, 49. (f) Chisholm, M. H.; Conroy, B. K.; Clark, D. L.; Huffman, J. C. *Polyhedron* **1988**, *7*, 903.
(53) Chen, L. X.; Jäger, W. H. G.; Niemcyzk, M. P.; Wasielewski, M. R. *J. Phys. Chem. A* **1999**, *103*, 4341.
(54) Sayama, K.; Hara, K.; Ohga, Y.; Shinpou, A.; Suga, S.; Tsukagoshi, S.; Abe, Y.; Arakawa, H. Thirteenth International Conference on Photochemical Conversion and Storage of Solar Energy. July 30 − August 4, 2000. Snowmass, Colorado. p W6−O-6.
(55) Sayama, K.; Hara, K.; Ohga, Y.; Shinpou, A.; Suga, S.; Arakawa, H. *New J. Chem.* **2001**, *25*, 200.
(56) Qu, P.; Zhao, J.; Ling, Z.; Shen, T.; Hidaka, H. *Colloids Surf. A* **1998**, *138*, 39.
(57) Gao, Y.; Kispert, L. D. Submitted to *J. Phys. Chem. B.*
(58) Hill, T. J.; Land, E. J.; McGarvey, D. J.; Schalch, W.; Tinkler, J. H.; Truscott, T. G. *J. AM. Chem. Soc.* **1995**, *117*, 8322.
(59) Lutz, M.; Szponarski, W.; Berger, G.; Robert, B.; Neumann, J. M. *Biochim. Biophys. Acta* **1987**, *894*, 423.